

Single Nanoporous Gold Nanowire Sensors

Zhu Liu and Peter C. Searson*

Department of Materials Science and Engineering, Johns Hopkins University, Baltimore, Maryland 21218

Received: November 29, 2005; In Final Form: January 5, 2006

Chemisorption from the gas or liquid phase can result in a measurable resistance change in a metallic material when at least one dimension is smaller than the mean free path for electrons. Here we report on the fabrication of single nanoporous gold nanowires and demonstrate that adsorption of an alkanethiol can be monitored in real time. Single nanowire devices were fabricated by *in situ* etching of Au_{0.18}Ag_{0.82} alloy nanowires in dilute nitric acid. The evolution of the porous structure was characterized by monitoring the resistance change and comparing to cross-sectional images. The feature size of about 10 nm is less than the mean free path for electrons in bulk gold, and hence the resistance is dominated by surface scattering. Adsorption of a monolayer of octadecanethiol onto the nanoporous gold nanowire results in a resistance change of about 3%. The sensitivity factor of 1.0×10^{-16} cm² is comparable to values reported for adsorption at ultrathin films.

Introduction

The quasi-one-dimensional geometry of nanowires makes them ideal for device applications based on the transport of charge, such as field effect transistors (FETs). Single nanowire FETs have been fabricated using semiconductor nanowires or carbon nanotubes as the channel with the contacts to each end of the wire serving as source and drain electrodes. Adsorption of charged species on the surface of the nanowire gives rise to a change in conductivity that can be exploited for sensing.¹

In the fabrication of chemical sensors in metallic systems, finite size effects can be exploited for transduction. In bulk metals, the resistance is dominated by lattice scattering. However, when the dimension d of a metallic conductor is smaller than the mean free path of electrons l_m then the resistance becomes dominated by scattering of electrons at the surface.² In this case, the electronic coupling of adsorbates to the conduction electrons can give rise to a change in resistance.

The mean free path for most metals is on the order of a few tens of nanometers, and hence surface scattering is significant in films where the thickness is less than l_m or in wires where the diameter is less than l_m . Ultrathin metal films have been exploited as sensors for detection of adsorbates from both the gas phase^{3–8} and the liquid phase.^{9–16} Resistance changes in ultrathin metal films have been used to monitor underpotential deposition^{9,12} and the adsorption of halide ions^{9–11} and alkanethiols.^{13–16}

In the fabrication of compact sensors based on surface scattering, the challenge is to provide a high surface area with a relatively small device footprint. In this paper we report on a single nanoporous gold nanowire sensor that exploits surface scattering in the solid ligaments of the porous structure for signal transduction. The nanoporous structure is formed by chemically etching the less noble component from a single-phase binary alloy containing a noble metal. For example, nanoporous gold (NPG) is formed when Ag is etched from a Au_xAg_{1-x} alloy.^{17–21} Surface diffusion of the gold during the etching process results

in coarsening of the gold to form solid ligaments with feature sizes ranging from nanometers to microns depending on the initial alloy composition and the etching conditions.

In previous work we demonstrated that NPG nanowires can be fabricated by a two-step technique involving electrochemical template synthesis of Au_xAg_{1-x} alloy nanowires followed by removal from the template and subsequent etching in nitric acid.²² NPG nanowires exhibit high surface-to-volume ratios and feature sizes that can be in the nanometer range. Furthermore, NPG nanowires exhibit a small footprint and hence are attractive for sensor applications. In this paper, we use *in situ* etching of Au_xAg_{1-x} alloy nanowires to fabricate single NPG devices and report on the resistance change associated with the adsorption of an alkanethiol.

Experimental Section

Figure 1 shows a schematic illustration of NPG nanowire synthesis and device fabrication. Briefly, Au_xAg_{1-x} alloy nanowires were fabricated by electrochemical template synthesis. After removal from the template and suspension in a suitable solvent, the nanowires were dispersed on a substrate and electrical contacts were formed using conventional photolithography. Finally, the silver was etched from the alloy to form nanoporous gold nanowires.

An anodic alumina film (Whatman) with a nominal pore size of 200 nm was used as the template for electrodeposition of the alloy nanowires. A 600-nm-thick Cu film evaporated onto one side of the template served as the working electrode in a three-electrode cell with a Pt mesh counter electrode and a Ag/AgCl (3 M NaCl) reference electrode ($U_{eq} = 0.200$ V vs SHE). Au_{0.18}Ag_{0.82} nanowires approximately 15–20 μ m long were deposited from a solution containing 100 mM AgKCN (Alfa Aesar, 99%), 20 mM AuKCN (Alfa Aesar, 99.99%), and 0.25 M Na₂CO₃ (Alfa Aesar, 99%), pH 13, at -1.2 V (Ag/AgCl).²² The average diameter was 360 ± 20 nm.

After deposition, the Cu film was stripped by etching in a solution of 0.3 M CuCl₂ (Alfa Aesar, 99%) and 0.1 M HCl (Fisher Scientific, ACS grade). The alumina template was then dissolved in 2 M NaOH for more than 2 h at 50–70 °C. After

* Author to whom correspondence should be addressed. E-mail: searson@jhu.edu.

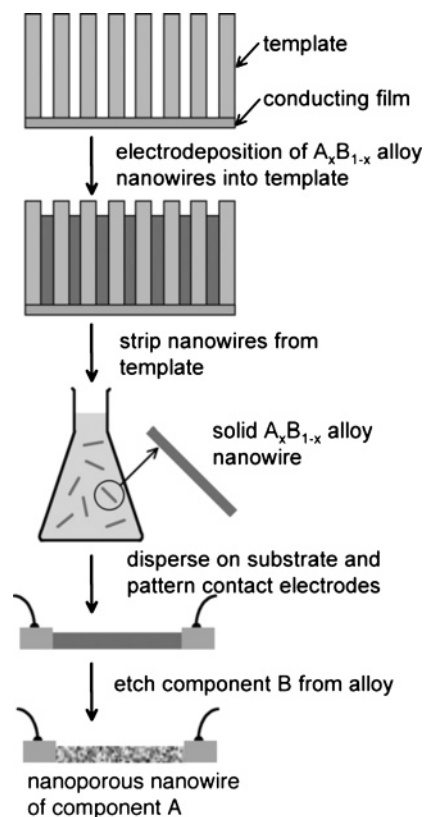


Figure 1. Schematic illustration of the fabrication of a single NPG nanowire device.

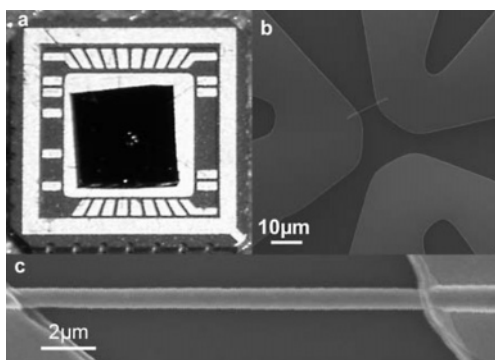


Figure 2. (a) Optical microscope image of a chip carrier with a single nanowire device, (b) plan view SEM image of a single nanowire showing the gold contacts patterned by photolithography, and (c) plan view SEM image of a NPG nanowire.

being washed in MilliQ water and centrifuged several times, the $\text{Au}_{0.18}\text{Ag}_{0.82}$ alloy nanowires were suspended in 2-propanol (Sigma Aldrich, ACS grade).

Single nanowire devices were fabricated on Si wafers with 500 nm oxide layers (Siliconquest) using photolithography and then assembled into a chip carrier by wire bonding. A drop of the nanowire suspension was dispersed on the wafer followed by drying in N_2 . Photoresist (S1827, Microchem) was spin-coated on the substrate at 3000 rpm and baked at 115°C . After the wafers were exposed using a mask with the lead pattern and developed, a 200–300 nm gold layer was evaporated onto the wafer. The photoresist was then removed, leaving the ends of the nanowires covered by the gold leads. The gold leads were then connected to a chip carrier (PLCC 28, Spectrum) by 25 μm in diameter gold wire. The length of the nanowires between the contacts was typically 5–8 μm . Figure 2 shows the chip carrier, the lead pattern, and a single nanowire.

The alloy nanowires were etched in situ to form the nanoporous structure. After assembling a single $\text{Au}_{0.18}\text{Ag}_{0.82}$ nanowire into a chip carrier, a drop of dilute (25 vol %) HNO_3 (EMD, ACS grade) was placed on the device. Etching was stopped by adding MilliQ water. The nanowire resistance was monitored during the etching process.

Resistance measurements were performed by scanning the current from -100 nA to 100 nA using a current source (Keithley 236) and measuring the corresponding voltage change (Keithley 2182 nanovoltmeter). The sensitivity of the resistance measurement was about 0.01Ω .

Cross sections of the NPG nanowires were prepared and imaged using a dual-beam focused ion beam (FIB) system (FEI NOVA dual-beam FIB). Cross sections were cut using a Ga ion beam current of 10 pA with a constant milling time of 30 s.

Experiments on thiol adsorption were performed in the following way. Approximately 5 mL of ethanol (Pharmca, ACS grade) was placed on the nanowire in the chip carrier. After it was ensured that there was no change in the resistance, octadecanethiol (ODT, $\text{CH}_3(\text{CH}_2)_{17}\text{SH}$, Sigma-Aldrich) was injected into the ethanol.

Results and Discussion

Fabrication of NPG Nanowires by In Situ Etching.

Nanoporous gold nanowires are relatively brittle, and processing steps such as washing and centrifugation can lead to fracture and hence short wire segments. In this work the NPG nanowires were formed by in situ etching of the silver from the $\text{Au}_{0.18}\text{Ag}_{0.82}$ alloy nanowires in dilute nitric acid, resulting in a device yield that was much higher than that obtained from first forming the NPG nanowires by etching in suspension.

The measured resistance of single 5–8 μm long $\text{Au}_{0.18}\text{Ag}_{0.82}$ nanowire devices was 10–50 Ω . The measured resistance is larger than the expected resistance of 1–2 Ω based on the physical dimensions and the resistivity for Au and Ag, indicating a contact resistance of about 5–25 Ω .

When the $\text{Au}_{0.18}\text{Ag}_{0.82}$ alloy nanowires were exposed to dilute nitric acid, the resistance increased with the etching time, as shown in Figure 3a. All resistance–time curves exhibited two characteristic regimes. On introduction of the dilute nitric acid, the resistance increased by a few ohms within the first minute. The resistance then remained relatively constant for 4–5 min, after which the resistance increased dramatically. Etching was stopped when the resistance was in the range of 100–500 Ω by rinsing with water. If etching was allowed to continue beyond this point, the resistance continued to increase, and eventually the wires broke, resulting in an open circuit. Figure 3b shows a control experiment where a pure Au nanowire was exposed to dilute nitric acid, illustrating that there is no change in resistance.

In Figure 3a, the resistance rapidly increases by 2.2 Ω in the first 20 s. The $\text{Au}_{0.18}\text{Ag}_{0.82}$ alloy nanowire was 6.5 μm in length and 360 nm in diameter. Taking an average resistivity of $2 \mu\Omega \text{ cm}$ ($\rho_{\text{Ag}} = 1.6 \mu\Omega \text{ cm}$ and $\rho_{\text{Au}} = 2.2 \mu\Omega \text{ cm}$), the resistance of the solid alloy nanowires is determined to be about 1.3 Ω . After 20 s etching, the resistance increases by 2.2 Ω to 3.5 Ω , equivalent to the resistance of a solid nanowire of the same length with a diameter of 217 nm (i.e. a cross-section of 0.36 of the original nanowire). In the absence of coarsening, complete etching of the silver would result in a cross-sectional area 0.18 of the original nanowire. Thus we can infer that about 78% of the silver is removed in the first 20 s. The extent of the plateau region where the resistance remains essentially constant is

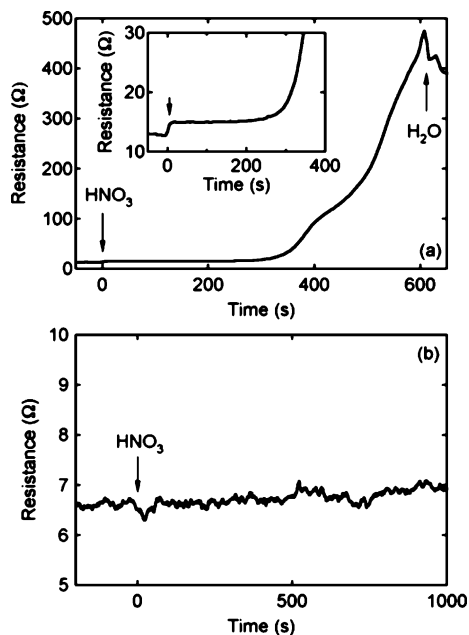


Figure 3. (a) Resistance change during in situ etching of a single $\text{Au}_{0.18}\text{Ag}_{0.82}$ nanowire in dilute HNO_3 with an initial resistance of 13Ω . The inset shows an expanded plot of the resistance during the initial stages of etching. (b) Resistance versus time plot for a pure Au nanowire in dilute HNO_3 .

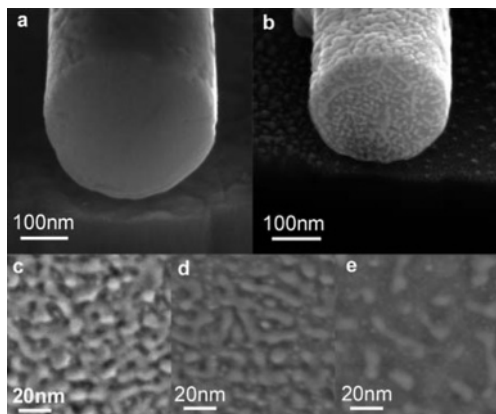


Figure 4. (a) SEM cross-section image of (a) a pure gold nanowire and (b) a NPG nanowire. Cross-section SEM images of $\text{Au}_{0.18}\text{Ag}_{0.82}$ nanowires after in situ etching in HNO_3 for (c) 1 min, (d) 5 min, and (e) 20 min.

dependent on the nitric acid concentration. In concentrated nitric acid, the resistance increases very rapidly to the break point, and hence the etching process is difficult to control. Thus by performance of the etching process in situ it is possible to control the morphology and resistance of the NPG nanowires

Characterization of the Porous Structure. Figure 4a shows a cross-section image of a $\text{Au}_{0.18}\text{Ag}_{0.82}$ alloy nanowire, illustrating that the nanowires are solid with a diameter of about 360 nm. Figure 4b shows a cross-section image of an NPG nanowire after etching, illustrating the characteristic structure of nanoporous gold. During the etching process the silver atoms are removed, leaving gold-rich regions. Diffusion of the gold atoms at the surface is relatively fast, resulting in coarsening of the structure. The coarsening of the remaining gold results in a significant decrease in the wire diameter, as can be seen from the scanning electron microscope (SEM) images.

Figures 4c–e show cross-section images of the porous structure after in situ etching in dilute nitric acid for 1, 5, and

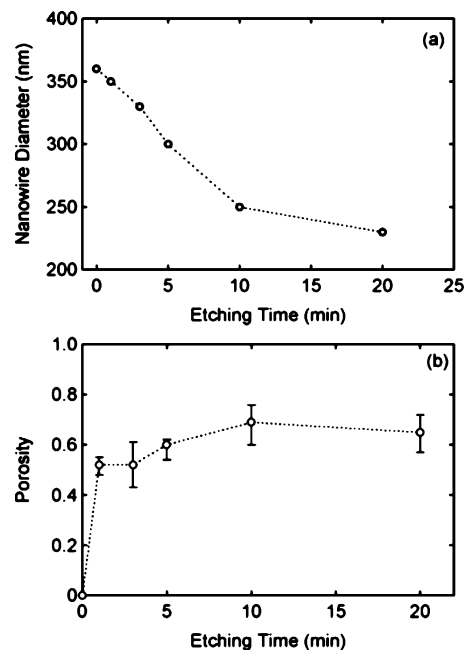


Figure 5. (a) Nanowire diameter versus etching time during in situ etching in dilute HNO_3 and (b) the porosity versus etching time determined from analysis of the cross-section SEM images.

20 min, respectively. After 1 min of etching, Figure 4c, the cross-section image shows that the nitric acid has penetrated to the center of the nanowire and that the morphology is relatively uniform. From Figures 4d and 4e, it is evident that the porosity continues to increase with etching time, indicating that Ag is still being removed from the nanowire.

Figure 5a shows the wire diameter plotted versus etching time, illustrating that etching and coarsening continue for the first 10 min of etching. After 20 min of etching, energy dispersive spectroscopy in the transmission electron microscope revealed that almost no Ag remained in the nanowire, indicating that the etching process is complete. The continued coarsening eventually results in fracture since both ends of the nanowire are constrained by the contact electrodes.

Figure 5b shows the porosity of the nanowires estimated from analysis of the cross-section images. The boundaries of the solid regions were first identified by thresholding the images and the porosity and then determined from the fractional area. This figure shows that the porosity increases dramatically during the first minute as a large amount of silver is etched from the alloy. Both etching and coarsening occur during the first 10 min. This is also evident from the fact that coarsening alone would result in a decrease in porosity. After 10 min of etching, both the diameter and the porosity exhibit a relatively small change, indicating that most of the Ag has been etched and that the rate of coarsening is significantly reduced.

We can compare the porosity at long times with the value estimated from the wire diameter in Figure 5a. After 20 min of etching the wire diameter is 230 nm. Assuming that all of the silver is etched from the alloy, then we estimate an average porosity of 0.56, which is good agreement with the value, 0.65 ± 0.08 , obtained from analysis of the image in Figure 4e.

We can now compare the resistance change during etching with the wire diameter and porosity. The SEM images show that during the first minute the nitric acid has penetrated to the center of the wires, producing a uniform morphology with a porosity of 0.53 ± 0.04 . As described above the resistance

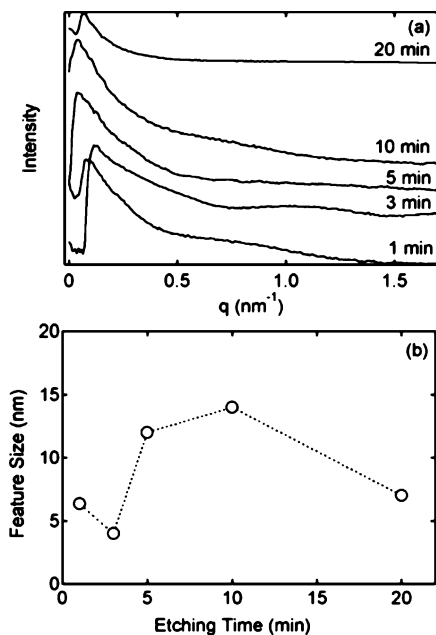


Figure 6. (a) Intensity versus q plot obtained from transformation of the cross-section SEM images. The etching time is indicated in the figure. (b) Characteristic feature size associated with the solid ligaments in the NPG nanowires plotted versus etching time.

change that occurs in the first 20 s corresponds to etching of about 78% of the silver. Taking into account that the diameter has decreased to 350 nm, the reduction in area corresponds to a porosity of 0.61, in reasonable agreement with the value obtained from the SEM image. After the initial increase, the resistance remains essentially constant for the next 4–5 min. During this time coarsening is relatively fast, resulting in a significant decrease in the diameter of the nanowires. The remaining silver is also etched during this time so that there is little change in the porosity. At longer times coarsening continues, ultimately resulting in fracture of the solid ligaments in the porous structure and hence a rapid increase in the resistance.

Analysis of the cross-section images can be used to obtain the average ligament size in the porous structure. Fast Fourier transforms (FFTs) of the cross-section images can be used to obtain the ligament size of the porous structure. Figure 6 shows intensity versus q plots obtained from two-dimensional FFTs of the cross-section images after thresholding. The peaks in the plots indicate the characteristic feature size in the nanoporous structure as a function of etching time. The mean free path for electrons in gold is about 50 nm,²³ significantly larger than the average ligament size of around 10 nm, as can be seen in Figure 6b. These dimensions are in good agreement with feature sizes seen in transmission electron microscope images (not shown).

Single NPG Nanowire Devices. Figure 7 shows the normalized resistance change for a single NPG nanowire on introducing 10 μL of 1 mM ODT. This concentration of ODT is in excess of the amount needed to form a self-assembled monolayer at the surface. The resistance increases by 3% over a period of about 1 min, corresponding to the time for the formation of a monolayer at a planar surface.²⁴ The response time and resistance change are comparable to values reported for thiol adsorption on ultrathin gold films.^{13–16} Although not demonstrated here, experiments on ultrathin gold films have shown that the initial resistance can be recovered by exposure to ozone and ethanol.¹⁵

This result demonstrates that the NPG nanowire consists of an interconnected network of ligaments with dimensions less

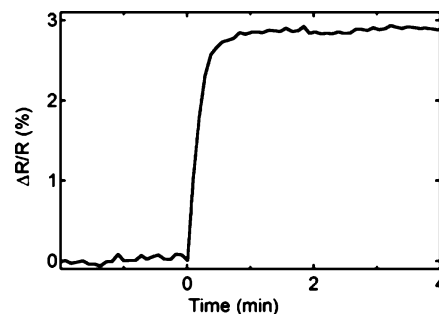


Figure 7. Normalized resistance change versus time for a single NPG nanowire on exposure to 10 μL of 1 mM ODT. Note that the ODT concentration was in excess of the amount needed to form a monolayer at the surface.

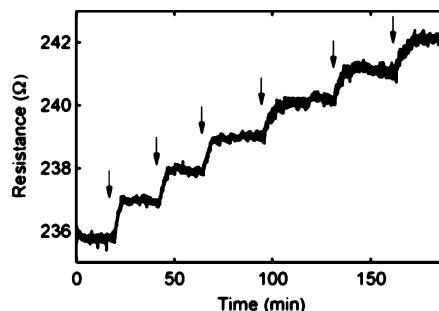


Figure 8. Resistance versus time for a single NPG nanowire device. The arrows indicate the injection of aliquots of 5×10^{-11} mol ODT.

than the mean free path of electrons. We note that the resistance of the NPG nanowires is typically 100–500 Ω , significantly larger than the contact resistance, and hence the resistance change is dominated by the change in surface scattering.

The change in resistance is related to the increase in diffusive scattering at the surface due to the presence of adsorbates. At an ideal surface, all electrons are specularly reflected (elastically scattered with no change in momentum in the direction of the electric field). The presence of adsorbates or other defects can lead to diffusive (inelastic) scattering of electrons that is associated with a change in momentum. Thus at a real surface, as long as the fraction of specularly reflected electrons is sufficiently large, then adsorption will introduce scattering centers that will increase the fraction of diffusively scattered electrons. If the dimensions of the solid are smaller than the electron mean free path such that the resistance is dominated by surface scattering, then adsorption can lead to a measurable change in resistance.

Figure 8 shows an experiment where small aliquots (5×10^{-11} mol) were sequentially injected into the ethanol on the chip carrier. The initial resistance of the nanowire is 236 Ω , and each aliquot results in a 1 Ω increase in the resistance. Figure 9 shows the resistance change plotted versus the ODT surface concentration. The surface concentration was determined from the amount of ODT at the onset of saturation of the resistance and taking monolayer coverage as 4.6×10^{14} cm^{-2} .²⁴

In experiments in the gas phase with ultrathin films, the resistance increases linearly with coverage and then either saturates or reaches a maximum that is dependent on the film thickness, the electron mean free path, and the binding energy of the adsorbate on the metal surface.²⁵ At the low coverage, the linear relationship can be expressed as

$$\left[\frac{d(\Delta R/R)}{d(dn)} \right]_{n \rightarrow 0} = \frac{Al_m}{d} \quad (1)$$

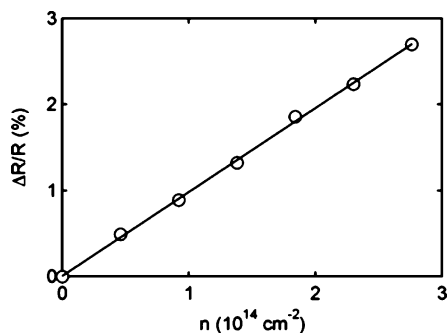


Figure 9. Normalized resistance change versus the surface concentration of ODT derived from Figure 8. Monolayer coverage corresponds to a surface concentration of $4.6 \times 10^{14} \text{ cm}^{-2}$.

where the $\Delta R/R$ is the normalized resistance change, n is the number of adsorbate molecules per unit area, d is the film thickness, and A is a constant. The slope of the linear region represents a characteristic parameter for a given system.

From Figure 9 we determine a slope of $1.0 \times 10^{-16} \text{ cm}^2$. In comparison, a slope of $0.2 \times 10^{-16} \text{ cm}^2$ has been reported for ODT adsorption on ultrathin gold films.¹⁴ A sensitivity factor of $2 \times 10^{-16} \text{ cm}^2$ has been reported for adsorption of CO on 10 nm Cu films, and a slope of $0.5 \times 10^{-16} \text{ cm}^2$ has been reported for adsorption of CO on 10 nm Ni films.²⁵ These results show that the single NPG nanowire devices have sensitivities comparable to relatively large area thin films.

Conclusions

Single NPG nanowire sensors were fabricated by in situ etching of $\text{Au}_{0.18}\text{Ag}_{0.82}$ alloy nanowires using simultaneous resistance measurements to monitor the etching process. We show that most of the silver is etched during the first 20 s and that subsequent coarsening and etching result in a significant decrease in the nanowire diameter. The final porosity of the devices is about 0.65. The characteristic feature size of the porous structure is about 10 nm, smaller than the mean free path of electrons in bulk gold so that the resistance is dominated by surface scattering. The performance of the nanowires as

sensors for adsorption of octadecanethiol resulted in a sensitivity of $1.0 \times 10^{-16} \text{ cm}^2$, comparable to values reported for adsorption at ultrathin films.

Acknowledgment. This work was supported by the JHU MRSEC (National Science Foundation Grant No. DMR05-20491).

References and Notes

- (1) Cui, Y.; Wei, Q. Q.; Park, H. K.; Lieber, C. M. *Science* **2001**, *293*, 1289–1292.
- (2) Sondheimer, E. H. *Adv. Phys.* **1952**, *1*, 1–42.
- (3) Chopra, K. L.; Bobb, L. C.; Francombe, M. H. *J. Appl. Phys.* **1963**, *34*, 1699–1702.
- (4) Persson, B. N. J. *Phys. Rev. B* **1991**, *44*, 3277–3296.
- (5) Persson, B. N. J. *J. Chem. Phys.* **1993**, *98*, 1659–1672.
- (6) Hein, M.; Schumacher, D. J. *Phys. D: Appl. Phys.* **1995**, *28*, 1937–1941.
- (7) Krastev, E. T.; Kuhl, D. E.; Tobin, R. G. *Surf. Sci.* **1997**, *387*, L1051–L1056.
- (8) Cabrera, A. L.; Garrido Molina, W.; Colino, J.; Lederman, D.; Schuller, I. K. *Phys. Rev. B* **1997**, *55*, 13999–14004.
- (9) Dickinson, T.; Sutton, P. R. *Electrochim. Acta* **1974**, *19*, 427–435.
- (10) Hansen, W. N. *Surf. Sci.* **1980**, *101*, 109–122.
- (11) Rath, D. L.; Hansen, W. N. *Surf. Sci.* **1984**, *136*, 195–216.
- (12) Hanewinkel, C.; Winkes, H.; Schumacher, D.; Otto, A. *Electrochim. Acta* **1997**, *42*, 3345–3349.
- (13) Zhang, Y.; Terrill, R. H.; Bohn, P. W. *J. Am. Chem. Soc.* **1998**, *120*, 9969–9970.
- (14) Zhang, Y.; Terrill, R. H.; Bohn, P. W. *Chem. Mater.* **1999**, *11*, 2191–2198.
- (15) Zhang, Y. M.; Terrill, R. H.; Bohn, P. W. *Anal. Chem.* **1999**, *71*, 119–125.
- (16) Fried, G. A.; Zhang, Y. M.; Bohn, P. W. *Thin Solid Films* **2001**, *401*, 171–178.
- (17) Pickering, H. W.; Wagner, C. J. *Electrochim. Soc.* **1967**, *114*, 698–706.
- (18) Forty, A. J. *Nature* **1979**, *282*, 597–598.
- (19) Li, R.; Sieradzki, K. *Phys. Rev. Lett.* **1992**, *68*, 1168–1171.
- (20) Yoon, J.; Chan, M. H. W. *Phys. Rev. Lett.* **1997**, *78*, 4801–4804.
- (21) Erlebacher, J.; Aziz, M. J.; Karma, A.; Dimitrov, N.; Sieradzki, K. *Nature* **2001**, *410*, 450–453.
- (22) Ji, C. X.; Searson, P. C. *J. Phys. Chem. B* **2003**, *107*, 4494–4499.
- (23) Tanner, B. K. *Introduction to the Physics of Electrons in Solids*; Cambridge University Press: Cambridge, U. K., 1995.
- (24) Schlenoff, J. B.; Li, M.; Ly, H. *J. Am. Chem. Soc.* **1995**, *117*, 12528–12536.
- (25) Wissman, P. *Tracts Mod. Phys.* **1975**, *77*, 1–96.